Observation and Structure Determination of an Oxide Quasicrystal Approximant

S. Förster,[1,*] M. Trautmann,[1] S. Roy,[2,†] W. A. Adeagbo,[1] E. M. Zollner,[1] R. Hammer,[1] F. O. Schumann,[1]
K. Meinel,[1] S. K. Nayak,[1,‡] K. Mohseni,[2] W. Hergert,[1] H. L. Meyerheim,[2] and W. Widdra[1,2]

[1]*Institute of Physics, Martin-Luther-Universität Halle-Wittenberg, D-06099 Halle, Germany*
[2]*Max-Planck-Institut für Mikrostrukturphysik, Weinberg 2, D-06120 Halle, Germany*
(Received 14 June 2016; published 24 August 2016)

We report on the first observation of an approximant structure to the recently discovered two-dimensional oxide quasicrystal. Using scanning tunneling microscopy, low-energy electron diffraction, and surface x-ray diffraction in combination with *ab initio* calculations, the atomic structure and the bonding scheme are determined. The oxide approximant follows a $3^2.4.3.4$ Archimedean tiling. Ti atoms reside at the corners of each tiling element and are threefold coordinated to oxygen atoms. Ba atoms separate the TiO_3 clusters, leading to a fundamental edge length of the tiling 6.7 Å.

Since their discovery in 1984, the aperiodic order of quasicrystals with a five-, eight-, ten-, or 12-fold symmetric diffraction patterns has fascinated researchers in many fields, e.g., crystallography, materials science, and mathematics. Whereas these quasicrystals were initially found only in intermetallic alloys [1–4], the concept of long-range quasicrystalline order was later extended to a variety of soft materials [5–11]. Recently, it has been shown that highly perfect quasicrystalline structures form even within 2D oxide layers [12].

Ultrathin films of the perovskite $BaTiO_3$, which are known to prefer cubic or distorted cubic structures in thin-film and bulk phases, convert into long-range ordered dodecagonal films when grown on a threefold Pt(111) substrate [12]. This dodecagonal structure, which develops in a two-dimensional wetting layer at the Pt interface, was the first oxide quasicrystal (OQC) discovered. The local atomic structure of the OQC, as determined by scanning tunneling microscopy (STM), exhibits arrangements of squares, triangles, and 30° rhombs, which share an edge length of 6.9 Å. From these three elements, a Stampfli-Gähler tiling is formed in the OQC [12–14]. Although this tiling has been atomically resolved by STM, it is expected that the tiling describes only one sublattice. The large interatomic spacing suggests that the Ti or the Ba sublattice is imaged by STM. However, only detailed knowledge of the positions of all atomic species within the building blocks of the OQC can unravel the bonding mechanisms leading to the aperiodic structure. From the experimental side it has been argued that the STM image determines the Ti sublattice [12]. In contrast, recent *ab initio* calculations propose an alternative structure with a Ba sublattice forming the Stampfli-Gähler tiling [15].

In this Letter, we report the observation of an oxide quasicrystal approximant that is closely related to the OQC. Approximants are periodic arrangements of the characteristic building blocks inherent to the quasicrystal [16]. For a given quasicrystal, various approximant structures differing in their structural complexity typically exist [17,18]. The reduced complexity of approximants due to their finite unit cell provides a route for the determination of structural elements that are also elements of the related quasicrystal. The translational symmetry in approximants allows for calculations that rely on periodic boundary conditions [19]. Here, the identification of an oxide approximant in close relationship to the OQC underlines the concept of quasi-crystallinity for 2D oxides. The approximant structure is a distorted $3^2.4.3.4$ Archimedean tiling [20,21]. It consists of structural elements based on squares and triangles with an edge length that agrees to within 10% of the fundamental edge length of the OQC. The ratio of triangles to squares in the approximant structure is 2, whereas it is increased to $(1 + \sqrt{3}) \approx 2.73$ in the aperiodic OQC. The common building blocks of approximant and OQC enable insights into the bonding schemes, leading to long-range aperiodic order in the $BaTiO_3$-derived thin film. The structure determination of the approximant by surface x-ray diffraction (SXRD) and density-functional theory (DFT) calculations, as presented here, is the important first step into a deeper understanding of the OQC.

Ultrathin films of $BaTiO_3$ were grown by rf magnetron sputter deposition as reported elsewhere [22]. The OQC was prepared by annealing ultrathin films of $BaTiO_3$ at temperatures above 1150 K in ultrahigh vacuum (UHV) [12]. At 1250 K the approximant structure develops in a rewetting layer of reduced $BaTiO_3$.

An atomically resolved STM image of the OQC approximant is shown in Fig. 1(a). The approximant exhibits a periodic structure with a nearly quadratic unit cell as marked by the solid red line. The STM image exhibits four atomic protrusions within the unit cell, which correspond to electron tunneling into unoccupied Ti $3d$ states as discussed later. Between adjacent unit cells we notice STM contrast variations that are caused by a 2.8-nm periodic
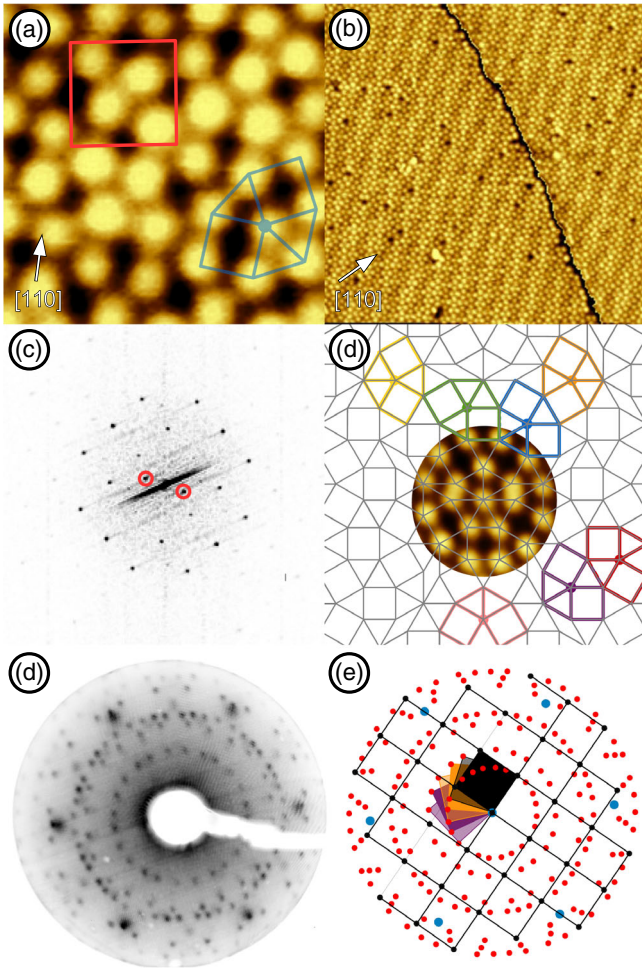
FIG. 1. (a) Atomically resolved STM image of the BaTiO$_3$-derived OQC approximant (4×4 nm^2, 0.3 nA, 1.0 V). The unit cell of the snub-square tiling is marked in red. The characteristic five-vertex element is marked in blue. (b) Large-scale image of the moiré structure of the approximant on Pt(111) (35×35 nm^2, 0.5 nA, -1 V). (c) Fourier transform of (b). The spots marked by red circles reveal the moiré periodicity. (d) Schematics of the quasicrystalline tiling with emphasis on the five-vertex elements therein. (e) LEED pattern of the OQC approximant on Pt(111) at 20 eV. (f) Assignment of the LEED spots to the six domains of the approximant.

moiré structure, which becomes more clear on a larger length scale as shown in Fig. 1(b). A Fourier transform of the STM image [Fig. 1(c)] confirms the nearly quadratic unit cell with lattice vectors of 12.9 and 13.1 Å enclosing an angle of 90.5°. Note that the moiré structure is a higher-order commensurate structure with respect to the Pt(111) substrate that can be described by a $\binom{27\ 10}{3\ 20}$ superstructure matrix. It leads to a moiré periodicity of 2.78 nm, which matches the experimentally observed value. The LEED pattern of the OQC approximant in Fig. 1(e) reveals the existence of six domains according to the $p3m1$ plane group symmetry of the substrate surface. From Fig. 1(e) a rotation of the shorter unit cell vector of the approximant

of 8° with respect to the $\langle 110 \rangle$ directions of Pt(111) has been determined. The simplified unit cell of the approximant as shown in Fig. 1(a) can be described by a superstructure matrix $\binom{27/5\ 2}{3/4\ 5}$ with respect to the Pt(111) surface. The four protrusions in the unit cell of Fig. 1(a) have an average distance of 6.7 Å. This large separation of the protrusions that deviates less than 10% from the fundamental length scale of the aperiodic OQC indicates that here the sublattice of a single element in the BaTiO$_3$-derived structure is imaged. The metallic behavior in electron tunneling suggests that the STM contrast is given by Ti 3d-derived states close to the Fermi level. Each Ti atom in the approximant structure has an identical local arrangement, with five neighboring Ti atoms forming the five-vertex structure as marked in blue in Fig. 1(a). In this way the Ti sublattice forms the well-known $3^2.4.3.4$ Archimedean tiling [20], also known as snub-square tiling, which was described 400 years ago by Kepler [21]. This tiling is the prototypical approximant structure of dodecagonal square-triangle tilings and has also been observed for soft-matter quasicrystals [7,8,11,23,24] as well as for intermetallic quasicrystals [17,25]. The unit cell of the snub-square tiling includes only two squares and four triangles as tiling elements. Hence, it is the approximant of the lowest possible structural complexity for dodecagonal quasicrystals. On the other hand, the five-vertex elements are dominant and characteristic units of the aperiodic Stampfli-Gähler tiling as indicated in Fig. 1(d).

For a structure determination that goes beyond the Ti sublattice structure observations with STM, SXRD experiments were carried out at beam line ID03 of the European Synchrotron Radiation Facility (ESRF) using a six-circle UHV diffractometer. Structure factor amplitudes $|F_{\text{obs}}(hk\ell)|$ were derived from integrated reflection intensities $I_{\text{obs}}(hk\ell) \propto |F_{\text{obs}}(hk\ell)|^2$ collected under total external reflection conditions of the incoming beam ($\lambda = 1.10$ Å) using a 2D pixel detector [26]. In total, 176 reflections of type ($hk\ell$) with $\ell \approx 0$ were measured, reducing to 43 symmetry-independent reflections after averaging over symmetry equivalent reflections (plane group $p2$) and equivalent reflections of different domains. Amplitudes of equivalent reflections agree to within 15% on average, which can serve as an estimate of the uncertainty. We note, however, that the refinement was carried out by treating all $|F_{\text{obs}}(hk)|$ with equal weight; i.e., the unweighted R_U was optimized [27].

The structure analysis was carried out by following classical procedures known from 3D crystallography [28]. Owing to their strong scattering amplitude, the Ba atoms can easily be identified in the (z-projected) 2D Patterson function $P(u, v)$ which is the Fourier transform of the $|F_{\text{obs}}(hk\ell)|^2$ as discussed for 3D and 2D systems [28,29]. Once the position of the ("heavy") Ba atoms is refined, giving a residuum of $R_U \approx 30\%$, the calculated difference charge density $\Delta\rho(x, y)$ between the calculated and the

experimental structure factors directly provides information about the location of the Ti sublattice. Ti atoms appear as positive maxima in $\Delta\rho(x,y)$, which are located approximately at the positions of the protrusions in the STM image. The positions of the barium and titanium atoms are used as the starting model for the least squares refinement. In this way—by excluding the O atoms—the refinement of the atomic positions yields an unweighted residuum (R_U) of 18%. This allows us to make the conclusion that the most important features of the structure are correctly modeled [28], i.e., that almost all calculated scattering phases $\alpha_{\text{calc}}(hk) = \pm\pi$ are correct. In an iterative way, the positions of the oxygen atoms can be derived by calculating $\Delta\rho(x,y)$. This refinement leads to a threefold coordination of the oxygen atoms around the titanium atoms with a best fit of $R_U = 14\%$. Finally, the calculation of the 2D charge density $\rho(x,y)$ is carried out, which is given by $\rho(x,y) = \sum F_{\text{obs}}(hk)\exp[-i2\pi(hx + ky)]$, with $F_{\text{obs}}(hk) = \pm|F_{\text{obs}}(hk)|$. Figure 2 shows $\rho(x,y)$ where four unit cells have been plotted to emphasize the tiling. Green, blue, and red circles represent Ba, Ti, and O atoms, respectively. In order to clarify the main features of the structure, the circles are directly located at the maxima of the charge density plot. It can be seen that each positive peak (solid lines) in $\rho(x,y)$ is directly associated to an atom. Negative peaks (dashed lines) also appear, 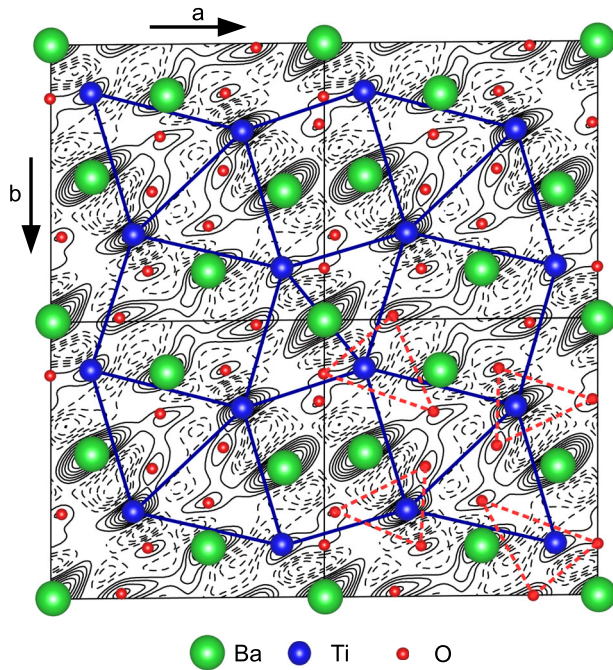which arise due to the use of a fractional data set [30]. We emphasize that the peak positions and their height do not exactly correspond to refined positions and the atomic number of the respective species. This is because of the limited number of Fourier coefficients, leading to truncation errors. Considerable static (anisotropic) disorder is directly observable in $\rho(x,y)$ as an elongation of the peaks along the [210] direction of the unit cell. We attribute this to the fact that the simplified $\left(\begin{smallmatrix} 27/5 & 2 \\ 3/4 & 5 \end{smallmatrix}\right)$ unit cell chosen in this analysis represents a projection of the structure related to the higher-order commensurate unit cell, which is 4×5 times larger. Thus, the static disorder is a result of an averaging over slightly different, albeit equivalent, positions of the atoms within the $\left(\begin{smallmatrix} 27 & 10 \\ 3 & 20 \end{smallmatrix}\right)$ into the $\left(\begin{smallmatrix} 27/5 & 2 \\ 3/4 & 5 \end{smallmatrix}\right)$ unit cell.

The SXRD analysis confirms that Ti atoms are forming the snub-square tiling observed by STM. The Ti atoms are surrounded by three oxygen atoms, approximately forming a triangle. The snub-square tiling of the OQC approximant is a strongly distorted square-triangle tiling, which includes two kinds of double triangular tiles. For the small double triangle, one Ba atom is located in the center, which coincides with the origin of the unit cell. Along the $\langle 1\bar{1}0\rangle$ direction of the unit cell, larger double triangles exist, for which Ba atoms decorate the outer sides of the edges. Two out of the five Ba sites exhibit a lower charge density in Fig. 2, indicating half occupancy of these positions. As a consequence, two different rectangles are spanned from Ti atoms, one with a large aspect ratio in which two Ba atoms are located next to the long edges, and one with a small aspect ratio for which the positions of the Ba at the long edges exhibit only half occupancy. The total stoichiometry of the structure can be written as $Ba_4Ti_4O_{10}$ per unit cell, when half occupancy is also assumed for the oxygen atoms next to the half-occupied Ba positions. This stoichiometry explains the OQC approximant formation under oxygen-reducing conditions from $BaTiO_3$ perovskite films and the observation of Ti^{3+} in the x-ray photoelectron spectroscopy [12].

Further insights come from DFT calculations by means of the Vienna *ab initio* simulation package [31–34]. The calculations were performed by using the PW91 GGA exchange correlation functional [35]. The calculated Pt lattice constant 3.92 Å is used to construct a 13.9×14.4 Å surface supercell of Pt(111). The whole supercell contains a slab consisting of an approximant layer and 4 Pt layers to simulate the substrate. The slabs are separated by a vacuum space of about 22 Å to prevent artificial interactions. Partial occupations such as those found experimentally cannot easily be taken into account. A formal stoichiometry of $Ba_5Ti_4O_{12}$ per unit cell is used instead.

The initial structural model uses the positions of the Ti atoms as determined by STM. In the first step, a freestanding approximant monolayer is considered, for which the dimension of the double Ti triangle in the unit cell has been fixed in order to determine the appropriate Ba and O atoms arrangement around it. The final positions of the

FIG. 2. SXRD-derived charge density $\rho(x,y)$ contour plot of four 2D unit cells of the OQC approximant. The snub-square tiling is indicated by the solid blue lines. Peaks in $\rho(x,y)$ are identified with Ba (green), Ti (blue), and O atoms (red). In the lower right part the threefold coordination of oxygen atoms around titanium atoms is emphasized by dashed triangles.
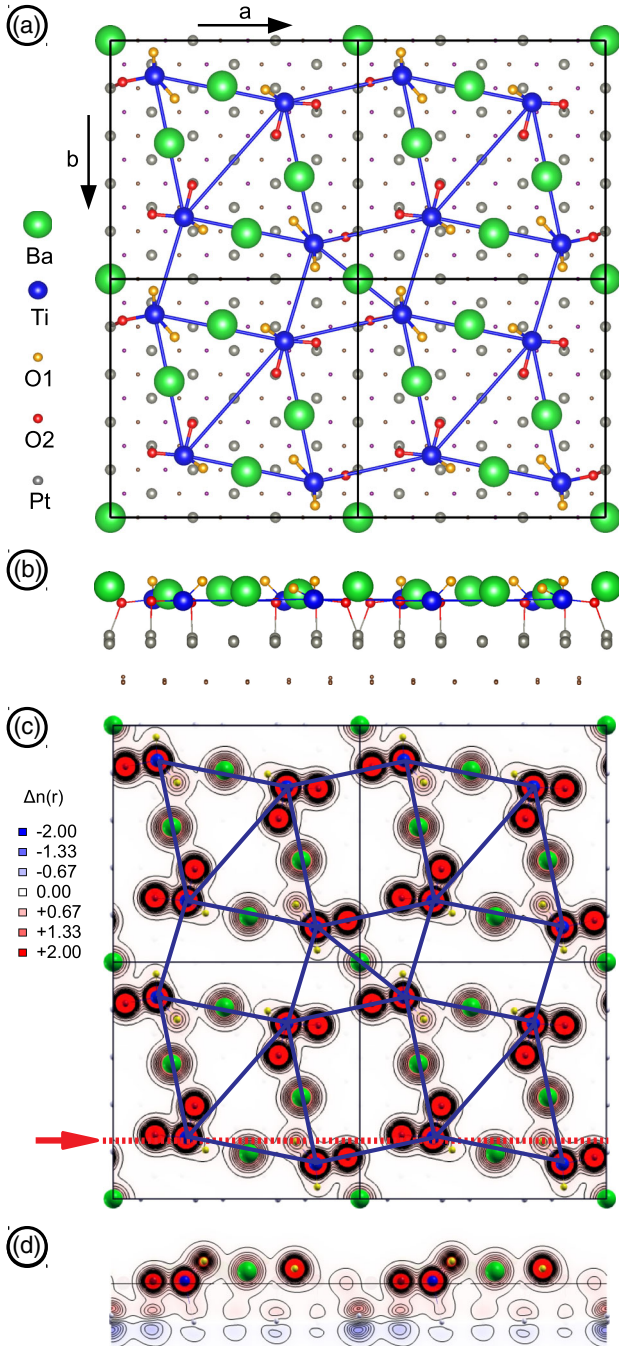
FIG. 3. Relaxed approximant structure on Pt(111) from *ab initio* calculations: (a) top view, (b) side view. Corresponding charge density distribution with superimposed real structure: (c) top view, (d) side view for a cut along the dashed line marked with the arrow in (c).

Ba and O atoms are reached if the forces on the atoms are less than 0.1 eV/Å. Practically, no vertical relaxation is found. The Ba atoms are located on the edges of the large double triangle and in the center of the small double triangle. The O atoms are bound to the Ti atoms. A stepwise constrained relaxation procedure followed for structure optimization on the Pt(111) substrate. In this

procedure, the first two layers of Pt are allowed to relax in the z direction. The oxygen atoms are always allowed to relax freely. Starting from the relaxed freestanding approximant structure, vertical relaxations of the Ba and Ti atoms are allowed. In the next step, Ba is allowed to relax in all directions, followed by a complete relaxation of the Ti atoms. The final relaxation of the Ti atoms leads to only small deviations from the experimental Ti positions and does not alter the arrangement of Ba and O atoms.

Figures 3(a) and 3(b) depict the final structure of the OQC approximant as a result of the *ab initio* calculations. The Ti atoms still reside in a plane but show a relaxation towards the Pt surface. The Ba atoms relax outwards; i.e., the Ba atoms are located above the Ti plane. A sizable vertical relaxation is obtained for the O atoms leading to two distinct species, which also gives rise to a different degree of hybridization of the O $2p$ bands with the $3d$ bands of Ti. The first species (O1) is located above the plane of the Ti network and shows a stronger hybridization with Ti as compared to the second (O2), which is bound to the Pt surface. As a result, the former average Ti-O bond length (1.78 Å) is smaller than for the second species (1.90 Å). We find six O atoms of both sorts in an arrangement that preserves a $p2$ symmetry. It should be noted that a change of the size of the double triangles of Ti will mainly influence the bonding of the O atoms, leading to a different number of O1 and O2 atoms.

The structural model recently proposed by Cockayne *et al.* for the OQC, snub-square tiling, and other approximants suggests ideal squares, equilateral triangles, and 30° rhombs decorated with Ba, Ti, and O atoms as building blocks for all tilings [15]. Dense TiO_3 networks can be generated such in different arrangements, in which holes of different sizes are filled with Ba atoms. Our model agrees in the height variations of the approximant structure caused by the inward relaxation of the Ti atoms and an outward relaxation of the Ba atoms. Furthermore, the Ti-O distances in the TiO_3 units can be reproduced. However, our observation of a pronounced distortion of the squares and triangles in the snub-square tiling as determined by SXRD, and the identification of a snub-square tiling based on the Ti sublattice rather than the Ba sublattice, questions the previous structure model of Cockayne *et al.* that was based on uniformly decorated tiles.

In conclusion, we report here on the observation of an approximant structure for the recently discovered 2D oxide quasicrystal. The periodic approximant is in general a well-established concept in the crystallography of quasicrystals, and its observation in the 2D oxide thin film highlights the applicability of universal quasicrystal concepts for the new class of perovskite-derived quasicrystals. Furthermore, it allows a simplified access to atomic and electronic structures within periodic boundary conditions and will enable the direct comparison of periodic and aperiodic structures with otherwise similar building blocks. STM and LEED measurements identify a distorted snub-square tiling for the approximant structure that is higher-order commensurate

with respect to the substrate. SXRD has determined the structure of the OQC approximant. Both SXRD and DFT provide evidence that the Ti sublattice forms the snub-square tiling. The OQC approximant is based on TiO_3 units, which include two different oxygen species, i.e., oxygen atoms that link to neighboring TiO_3 units via Ba atoms and inward-relaxed oxygen atoms that bind to the substrate.

[*]stefan.foerster@physik.uni-halle.de

[†]Department of Physics and Astrophysics, University of Delhi, Delhi-110007, India.

[‡]Department of Materials Science and Engineering, University of Connecticut, Connecticut, USA.

[1] D. Shechtman, I. Blech, D. Gratias, and J. W. Cahn, Phys. Rev. Lett. **53**, 1951 (1984).

[2] N. Wang, H. Chen, and K. H. Kuo, Phys. Rev. Lett. **59**, 1010 (1987).

[3] L. Bendersky, Phys. Rev. Lett. **55**, 1461 (1985).

[4] T. Ishimasa, H. U. Nissen, and Y. Fukano, Phys. Rev. Lett. **55**, 511 (1985).

[5] T. Dotera, Isr. J. Chem. **51**, 1197 (2011).

[6] X. Zeng, G. Ungar, Y. Liu, V. Percec, A. E. Dulcey, and J. K. Hobbs, Nature (London) **428**, 157 (2004).

[7] K. Hayashida, T. Dotera, A. Takano, and Y. Matsushita, Phys. Rev. Lett. **98**, 195502 (2007).

[8] D. V. Talapin, E. V. Shevchenko, M. I. Bodnarchuk, X. C. Ye, J. Chen, and C. B. Murray, Nature (London) **461**, 964 (2009).

[9] J. Mikhael, J. Roth, L. Helden, and C. Bechinger, Nature (London) **454**, 501 (2008).

[10] S. Fischer, A. Exner, K. Zielske, J. Perlich, S. Deloudi, W. Steurer, P. Lindner, and S. Förster, Proc. Natl. Acad. Sci. U.S.A. **108**, 1810 (2011).

[11] J. Zhang and F. S. Bates, J. Am. Chem. Soc. **134**, 7636 (2012).

[12] S. Förster, K. Meinel, R. Hammer, and W. Widdra, Nature (London) **502**, 215 (2013).

[13] P. Stampfli, Helv. Phys. Acta **59**, 1260 (1986).

[14] F. Gähler, in *Quasicrystalline Materials* (World Scientific, Singapore, 1988).

[15] E. Cockayne, M. Mihalkovic, and C. L. Henley, Phys. Rev. B **93**, 020101(R) (2016).

[16] A. I. Goldman and K. F. Kelton, Rev. Mod. Phys. **65**, 213 (1993).

[17] H. Chen, D. X. Li, and K. H. Kuo, Phys. Rev. Lett. **60**, 1645 (1988).

[18] M. Conrad and B. Harbrecht, Chem. Eur. J. **8**, 3093 (2002).

[19] V. Elser and C. L. Henley, Phys. Rev. Lett. **55**, 2883 (1985).

[20] B. Grünbaum and G. C. Shephard, Math. Mag. **50**, 227 (1977).

[21] J. Kepler, *Harmonices Mundi* (Linz, 1619).

[22] S. Förster and W. Widdra, Surf. Sci. **604**, 2163 (2010).

[23] M. N. van der Linden, J. P. K. Doye, and A. A. Louis, J. Chem. Phys. **136**, 054904 (2012).

[24] H. Pattabhiraman, A. P. Gantapara, and M. Dijkstra, J. Chem. Phys. **143**, 164905 (2015).

[25] S. Kashimoto, A. Kocjan, Z. Jaglicic, S. Jazbec, H. Iga, T. Ishimasa, and J. Dolinsek, Phys. Rev. B **84**, 224201 (2011).

[26] C. M. Schleptüz, R. Herger, P. R. Willmott, B. D. Patterson, O. Bunk, Ch. Brönnimann, B. Henrich, G. Hülsen, and E. F. Eikenberry, Acta Crystallogr. Sect. A **61**, 418 (2005).

[27] The unweighted residual (R_U) is defined as $R_U = \sum ||F^{\mathrm{obs}}| - |F^{\mathrm{calc}}|| / \sum |F^{\mathrm{obs}}|$. The summation runs over all data points.

[28] M. J. Buerger, *Kristallographie* (Walter de Gruyter, Berlin, 1977).

[29] H. L. Meyerheim, A. Ernst, K. Mohseni *et al.*, Phys. Rev. Lett. **108**, 215502 (2012).

[30] H. L. Meyerheim, Habilitation thesis, Ludwig-Maximilians-Universität, 1995.

[31] G. Kresse and J. Hafner, Phys. Rev. B **47**, 558 (1993).

[32] G. Kresse and J. Hafner, Phys. Rev. B **49**, 14251 (1994).

[33] G. Kresse and J. Hafner, J. Phys. Condens. Matter **6**, 8245 (1994).

[34] G. Kresse and J. Furthmüller, Comput. Mater. Sci. **6**, 15 (1996).

[35] J. P. Perdew, K. Burke, and Y. Wang, Phys. Rev. B **54**, 16533 (1996).